# Maximum-Likelihood Estimation: A Mathematical Model for Quantitation in Nuclear Medicine

Stefan P. Müller, Marie Foley Kijewski, Stephen C. Moore, and B. Leonard Holman

*Department of Radiology, Harvard Medical School and Brigham and Women's Hospital, Boston, Massachusetts; Abteilung Nuklearmedizin, Universitaetsklinikum Essen, Federal Republic of Germany; and Department of Biomedical Engineering, Worcester Polytechnic Institute, Worcester, Massachusetts*

In a simulation study, we investigated the limitations of quantitation in nuclear medicine using a maximum-likelihood (ML) estimation model. We estimated activity, size, and position of a disk-shaped object on a circular, uniform background of unknown activity. The parameter estimates were unbiased, and their standard error was proportional to the square root of the total image counts. The estimates of object activity and size were strongly (negatively) correlated; the position estimates, however, were not correlated with estimates of any other parameters. This implies that a priori knowledge of object location does not improve precision. The minimal model of quantitation tasks should incorporate unknown object activity and size as well as unknown background activity. The ML estimation procedure was used to investigate the trade-off between resolution and sensitivity in gamma camera collimator design. The results implied that for complex tasks such as the multiparameter estimation task investigated here, optimum performance is achieved at a better resolution than that previously found optimal for detection of a well-specified object in a known background.

**J Nucl Med 1990; 31:1693–1701**

P rogress in the development of new radiopharmaceuticals has stimulated interest in the measurement of parameters of metabolic, physiologic, and receptor function from images of the tracer distribution obtained with positron emission tomography (PET) or single-photon emission computed tomography (SPECT). Many structures of interest (e.g., tumors, myocardium, cerebral cortex, brain nuclei) are small relative to the spatial resolution provided by current imaging systems, i.e., 5-10 mm full-width-at-half-maximum (FWHM) for PET and 10-25 mm FWHM for SPECT (1). Quantification is difficult for this reason. Because of the limited spatial resolution, the counts from the structure of interest are spread over a larger area in the image, and the peak activity is reduced. Consequently, the activity will be systematically underestimated until the size of the object approaches three times the FWHM of the point-spread function (PSF) of the imaging system (2-4). Dividing the measurements by a "recovery coefficient" (the ratio of measured activity to true activity) has been proposed as a method of correcting this bias (3). This correction, however, requires a priori assumptions about the size of the structure of interest (3). In addition, counts from the adjacent background are included in the region of interest (ROI) and contaminate the measurement; this error cannot be corrected by recovery coefficients (4,5). For these reasons, measurements obtained by ROI or peak methods from resolution-limited images, although possibly clinically useful, are not statistically optimal estimates of the true physical quantities in the object of interest.

Quantitation is only one of the tasks routinely performed on medical images. Other tasks, such as feature detection, size discrimination, or shape recognition, have been studied extensively using models based on signal detection theory (6,7). The process of deciding, for example, whether or not a structure is present, can be mathematically modeled in a statistically optimal sense as a lesion-matched filter. This leads to the concept of the "ideal observer," which uses all the information in the image and provides an upper limit on performance in a given task. The performance of the ideal observer can be described by the task signal-to-noise ratio (SNR), which is determined by the properties of the imaging system and by the characteristics of the task. SNR has been shown to predict human performance in a variety of different tasks and under a wide range of imaging conditions. Human performance is typically lower than the ideal by a factor of about two (8-13). This model, however, is not applicable to multiparameter estimation tasks, such as quantitation in nuclear medicine, in which the dependence of the image on the parameters is nonlinear.

We propose to model quantitation of physical quantities as a parameter estimation problem in which the parameters are the quantities of interest, such as the size, location, and activity within a structure. This approach allows us to determine the relationships between physical properties of the imaging system, such as spatial resolution and noise, and performance in quantitative imaging tasks with several unknown parameters. Our goal is to establish a realistic model of quantitation which transcends the limits of the linear "ideal observer" model and allows a formal assessment of these complex nonlinear tasks.

Statistically optimal estimation methods have been extensively used in fields such as radar and communications (7). To estimate a parameter from a set of observed data, a model must be formulated which expresses the parameters in terms of the measured data. For data without errors, the deviation between the model and the data vanishes when the true parameter is used in the model. To estimate the parameter in the presence of statistical errors, a figure-of-merit is needed which describes the agreement between the model and the observed data for a given choice of the parameter value. To obtain the "best" estimate this figure-of-merit must be maximized. A figure-of-merit which is widely used is the maximum-likelihood (ML) criterion, by which the deviation between the model and the data is described in terms of the error distribution of the observed data. The "best" parameter estimate in the ML sense has the highest statistical likelihood to represent the true parameter in the data (7,14-17). For high SNR data, ML estimates are unbiased, have minimum variance (efficiency), and approach the true parameter value for large sample sizes (consistency); no other estimation rule yields more information about the parameters (sufficiency) (7). ML estimation is also related to the concept of the likelihood ratio used in signal detection theory (6,7,13) and has been applied to image resolution (18), tracer kinetic modeling and curve fitting (14,19,20), and tomographic reconstruction (21). Carson (2) used ML reconstruction to calculate the activity within ROIs whose shape, size, and position was known a priori.

In the present study, we investigate the properties of a ML estimator as a model of the quantitation problem for various physical conditions to derive the fundamental limitations of quantitation from nuclear medicine images and give an example of applying the ML estimation model to collimator optimization for quantitation.

## METHODS

### Estimation Model

We will use the ML criterion to fit an analytical model, $M(\bar{p})$, of the image as a function of the parameter vector, $\bar{p}$,

to the measured image. $M(\bar{p})$ is a vector whose elements are the pixels in the image. The model used in the work reported here incorporates a disk-shaped object surrounded by a uniform background. The parameters to be estimated are disk activity ($a_D$), radius ($r_D$), and position ($x_O$, $y_O$) and background activity ($a_{BG}$); background size and location are assumed known. The analytical model includes blurring by a Gaussian PSF with resolution (variance) of $\sigma^2$ and truncation of the background to a uniform circular area of radius $r_{BG}$ surrounding the object.

The likelihood that a given set of parameters, $\bar{p}$, for a given object has resulted in a particular measured image can be expressed in a statistical sense in terms of the underlying error (noise) distribution. The probability of an observed photon count rate is described by the Poisson distribution. For more than 15 detected counts, however, the Poisson distribution can be approximated by the more tractable normal distribution. For stationary white Gaussian noise, the individual pixel errors due to the statistical fluctuation of the image data are independent. The covariance matrix of these errors, therefore, is diagonal and the estimation task reduces to least squares estimation. In images reconstructed from projections by filtered backprojection, however, these errors are correlated and simple least-squares estimation does not fulfill the ML criterion. The correlations are described by the covariance matrix, C, which for stationary noise is the Fourier transform of the noise-power spectrum (NPS) (22-24). The single-pixel probability for the parameter vector, $\bar{p}$, can therefore be described by a multivariate normal distribution, and the likelihood, L, of $\bar{p}$ for the entire measured image, I, is given by the product of all the pixel probabilities:

$$L(\bar{p}) = (2\pi)^{-n/2} |C|^{-1/2}$$

$$\exp\left\{-\frac{1}{2} [I - M(\bar{p})]^T C^{-1}[I - M(\bar{p})]\right\}, \quad (1)$$

where n is the number of pixels. Instead of maximizing the likelihood function $L(\bar{p})$ itself, the negative logarithm is usually minimized. Eliminating all expressions which do not depend on the parameters leaves the following objective function, X, to be minimized:

$$X(\bar{p}) = [I - M(\bar{p})]^T C^{-1}[I - M(\bar{p})]. \quad (2)$$

The noise in the image can be made uncorrelated by filtering with the inverse Fourier transform of the reciprocal of the square foot of the NPS, a procedure known as "prewhitening" (7,25). Essentially, each point of the residual vector, [I-M($\bar{p}$)], is weighted inversely by the expectation value of the noise at the corresponding point in frequency space, i.e., the square root of the NPS. One might expect singularities in the prewhitening filter, given the theoretical form of the image NPS (23), which contains zero-valued components at low frequencies. Non-zero, low-frequency components have, however, been reported in spectra measured from transmission and emission computed tomography scanners (22,24,26). We have shown that these components can result from two-dimensional aliasing due to the discrete representation of the reconstructed image (24), and nonstationary of the projection NPS (22). After prewhitening, the image noise is uncorrelated and least squares estimation using the prewhitened model fulfills the ML criterion. Because the image has been modified by the

prewhitening operation, the model must be similarly altered. Assuming no zero-valued noise-power components, we obtain for the prewhitened model:

$$X(\bar{p}) = [F^{-1}\{F\{I\}\ NPS^{-1/2} - F\{M(\bar{p})\}\ MTF\ NPS^{-1/2}\}]^2, \quad (3)$$

where F denotes the Fourier transform and $F^{-1}$ its inverse. The product $MTF\ NPS^{-1/2}$ is the square root of the noise-equivalent quanta spectrum (NEQ), i.e., the spatial frequency distribution of the signal-to-noise ratio. This function is widely used to describe imaging systems (13,26–28).

The minimum of the objective function, $X(\bar{p})$, cannot be found analytically because it is nonlinear in the parameters. We use an iterative nonlinear fitting algorithm (29) which has been found to perform well even in the presence of large residuals, i.e., when the minimum of $X(\bar{p})$ is much larger than zero (30). The expression for the disk model in the frequency domain is:

$$F\{M(\bar{p})\} = \left\{(a_D - a_{BG}) \frac{r_D J_1(2\pi r_D f_r)}{f_r} \exp[-2\pi i(x_0 f_x \right.$$

$$\left. + y_0 f_y)] + a_{BG} \frac{r_{BG} J_1(2\pi r_{BG} f_r)}{f_r}\right\} \frac{\exp(-2\pi^2\sigma^2 f_r^2)}{NPS(f_x, f_y)^{1/2}}, \quad (4)$$

where $f_x$, $f_y$, and $f_r$ denote rectilinear and radial frequency-space coordinates. The analytical model in the parameters to be estimated ($a_D$, $r_D$, $x_0$, $y_0$, and $a_{BG}$) is shown as the Fourier transform of an expression involving Bessel functions of the fixed kind, the Gaussian MTF with standard deviation $\sigma$, and the NPS of the imaging system.

There exists a unique, invertible relationship between the spatial and frequency domains; it is, therefore, equivalent to perform the fit either in real space or in frequency space (7). We elected to perform the entire fitting operation in frequency space because of the simplicity of the expression in Equation 4 compared to its inverse Fourier transform.

In order to exclude effects due to potential cumulative roundoff errors, we used double-precision arithmetic for the fitting subroutines as well as for all function and gradient calculations. The Fourier transform and prewhitening operations, which are outside the fitting process, were computed in single precision. All fits were calculated to single precision convergence using the convergence criteria proposed by Dennis (29). This implies that further iterations would not yield statistically significant changes in the likelihood function (17). Fitting to the convergence tolerance for double precision did not noticeably change the results but required substantially longer computation times. All calculations were performed on a Micro VAX II minicomputer (Digital Equipment Corp., Maynard, MA).

## Simulation Experiments

Three sets of simulation experiments were performed. The first studied estimation of parameters from images in which the noise was uncorrelated (white). White noise characterizes planar gamma-camera images. The purpose of this study was to determine the relationships between performance of an optimal estimator in quantitation tasks and the basic physical properties of the imaging system, i.e., spatial resolution and level of noise. The performance of the ML estimator is compared to that of the familiar ROI-based estimation procedures. The purpose of the second set of experiments was to validate

the ML estimation procedure in the presence of the negatively correlated noise that characterizes images, such as those from SPECT systems, that are constructed from projections. For these images, the estimation procedure was applied to the prewhitened images. The validity of the ML estimation procedure in tomographic noise was shown by its equivalence to estimation from the raw projection data, in which the noise was white. The third set of experiments applied these methods to a practical design problem, determining the optimal size of collimator holes. Here resolution and noise are coupled, i.e., decreasing hole size simultaneously improves resolution and increases the level of noise. This implies that there is an optimal configuration for a particular imaging task.

## Estimation in White Noise

For our Monte Carlo simulation, we generated images with disk activity twice the background activity. To approximate the magnitude of the expected noise level in a scintigram, stationary, white, Gaussian-distributed noise corresponding to the average count level in the image was added to each pixel in the real-space image. We used linear congruential random generators with shuffling and a rejection technique to generate a Gaussian distribution (17). For all experimental conditions which were directly compared, we used the same random sequence.

The covariance matrix was computed from the true parameter values $\mu_i$ and $\mu_j$ and from the parameter estimates pi and $p_j$ from n=200 samples. The elements of the covariance matrix are given by:

$$C_{ij} = \sum_I^n (p_i - m_i)(p_j - m_j). \quad (5)$$

From this we calculated the standard error of each parameter and the correlations between pairs of parameters. Furthermore, to distinguish between random errors and bias, the accuracy, defined as the percent deviation of the mean of the estimates from the true parameters, and the precision, defined as the percent standard deviation about the mean of the estimates, were calculated for all parameters. We tested the assumption of normal distribution of the parameter estimates using the Kolmogorov-Smirnov test (17). To test for trends, we calculated the average residuals (deviations between the model and the data) and the average residual power spectrum from the residuals at the solution for each image. The parameter variance calculated from a finite number of replications becomes more stable as the number of replications increases. In a preliminary experiment to determine the number of replications necessary to ensure a good estimate of the parameter variance, we simulated 40,000 images of a disk with a diameter equal to the FWHM resolution. We calculated the standard deviation of the estimated parameters from 100 samples of 5 to 400 replications to determine the number of replications subsequently used in the study. The dependence of the standard error on the number of replications was determined by log-log linear regression. Unless stated otherwise, 200 images were used in subsequent experiments. In preliminary experiments, we had varied the object location within the background area and had not found an influence on the parameter estimates. Therefore, the object position was kept constant near the center of the background for all simulation experiments.

To study the dependence of standard error on image counts, we varied the total number of counts in the image from $10^3$ to $10^9$ for two resolution values: 4 and 6 pixels FWHM. For these experiments, disk diameters ranged from 4 to 16 pixels and the background diameter was 20 pixels. These fits were performed on 32×32 image matrices; all other experimental conditions used 64×64 pixel image representations. The standard error was plotted versus the number of counts in the image on a log/log scale and again the slope determined by linear regression.

Of special interest in nuclear medicine is quantitation of activity in objects small compared to the system resolution. We simulated high ($10^6$) count images for disk diameters ranging from 0.7 to 3 times the FWHM of the Gaussian point-spread function; the FWHM was 6 pixels and the background diameter 40 pixels. For the same set of images, estimates of regional activity were also calculated as the average over and the peak within a ROI corresponding in size and location to the disk. To study the potential of quantification in smaller structures, we also generated very high SNR images ($10^8$ counts) for disks of diameters 0.2 to 1 times the FWHM.

In detection experiments, it has been shown that observer performance is reduced when the location of the feature is unknown to the observer ($10,11,31,32$). We compared the performance of the ML-estimator under these circumstances to a three-parameter estimation problem in which the position of the feature was known. We used disk diameters ranging from 3 to 16 pixels on a background of 40 pixels diameter, a FWHM of 8 pixels, and $10^7$ counts in the image. The parameter means for activity, size, and background were compared to those from the five-parameter model using the paired t-test; the parameter variances were compared using Student's f-test ($15,16$).

### Estimation in Tomographic Noise

To demonstrate that estimation from the prewhitened image is equivalent to estimation from the corresponding projection set, we generated 128 projections of the disk model with 128 projection elements using the projection-slice theorem ($33$). We added Gaussian-distributed white noise of constant variance to each projection element as described above and reconstructed on a 64×64 matrix by the convolution-backprojection algorithm, using an unwindowed ramp filter ($34$) and linear interpolation. Each image was 'prewhitened' to remove the correlations in the image noise using a filter based on the NPS described by Kijewski and Judy ($24$). We then estimated from the prewhitened images disk activity, size, and background activity. We also estimated the parameters directly from the projection data by fitting the model of the projection data in the parameters—as described by the projection-slice theorem—to the projection data where the noise is uncorrelated and no prewhitening is required. We compared the performance of both methods for a disk activity twice that of the background and disk diameters ranging from 4.8 to 28 pixels for a FWHM of 6 pixels and a background diameter of 40 pixels.

### Optimization of a Collimator for Estimation of Regional Activity

To optimize a collimator for estimation from planar images, we incrementally varied the resolution. The count efficiency ($10^7$ counts at a FWHM resolution of 6.0 pixels) was proportional to the square of the resolution ($35$), disks with diameters ranging from 8 to 24 pixels for a fixed background diameter of 40 pixels were estimated. To ensure that our findings were not affected by real-space truncation of the background area (Gaussian PSF) or changes in the sampling of the object, we performed the same calculations with disk diameter fixed at 12 pixels while background diameter varied from 24 to 48 pixels. The optimal resolution was defined as that which resulted in the minimal standard error for the estimate of the parameter of interest as calculated from a 4th-order polynomial fit (the lowest order fit to give a correlation coefficient of 1.0).

## RESULTS

As expected, the standard deviation of the precision of the estimates derived from the simulations and the bias decreased with the inverse square root of the number of replications; the slope of the log/log representation was $-0.53$ with a correlation coefficient of $r^2 > 0.99$ for the activity and the size estimates. The estimates of the object activity, radius and background activity as well as the position estimates were normally distributed (Kolmogorov-Smirnov test, $p < 0.05$). Therefore, confidence limits for the estimated parameters can be calculated based on the normal distribution, and the paired t-test and F-test are appropriate to analyze the results. The average residuals were random by visual inspection, and the average residual power spectrum was constant for images with white noise. After prewhitening the tomographic images and fitting to the appropriate prewhitened model, the residual power spectrum was, again, constant, as were the residuals after estimation from the projections.

For fixed resolution and disk diameter, the standard error of the activity estimate was also inversely proportional to the square root of the total number of counts in the image over a wide range of counts; the slope in the log/log representation ranged from $-0.49$ to $-0.52$ with a correlation coefficient $r^2 > 0.99$.

In the $10^6$ count images, the accuracy of the ML estimator exceeded the precision for all parameters by about an order of magnitude over the entire range of disk sizes. We will, therefore, report the total standard error to characterize the estimator in the remaining simulation experiments. For $10^6$ image counts, the accuracy of the ML estimate of activity was superior to the conventional ROI and peak estimates, both of which are heavily biased; the precision, however, was worse (Fig. 1).

Although the activity and size estimates were of primary interest, examination of estimates of other parameters and the correlations between pairs of them was enlightening. The standard errors of the estimates of disk activity and disk diameter were of similar order, while the error on the position estimates was of the same order of magnitude as the bias of the size and activity estimates. For all situations studied we found a
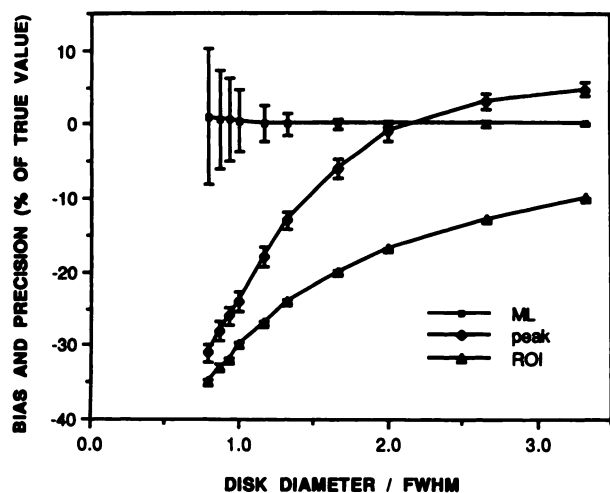
**FIGURE 1**
Precision and accuracy of ML, ROI, and peak estimates of disk activity as a function of the ratio of disk diameter to FWHM of the PSF in a $10^6$ count image. Accuracy is expressed as a percentage of the true value, precision (error bars) as % s.d.

negative correlation coefficient r of $-0.6$ to $-0.9$ between the activity and the size estimates, while the correlation of either activity or size with position was always less than $\pm$ 0.25. The standard error of the background estimate is largely dependent on the size of the background relative to that of the disk; as the disk diameter approaches the background diameter, the error of the background estimate and the correlation with the activity estimate increase. The standard errors of the activity and size estimates increased rapidly with decreasing object size, attaining a value of about 15% at a disk diameter of 0.7 times the FWHM resolution in a one-million-count image. Even at a 100-fold increase in the number of image counts, unrealistic for clinical images, only slightly smaller lesions can be estimated with the same standard error (Fig. 2).

Comparison of the parameter estimates for known and unknown location revealed no significant difference in mean value (paired t-test, p<0.05). In only 2 of 48 comparisons, the f-test indicated a significant difference (p<0.05) in variance of the estimates from the three-parameter fits compared to the five-parameter fits. This result does not suggest a statistical difference, since falsely significant differences must be expected for multiple comparisons. There also was no significant difference between estimation from the prewhitened tomographic images and from the projection data (Fig. 3).

Figure 4 shows the standard errors of the estimates of disk activity and disk diameter as a function of system resolution. There is a different optimum for the trade-off between resolution and sensitivity for the sizing and the activity estimation task. For all conditions, these slowly varying functions were well described by a 4th-order polynomial (r=1.00). We analytically calculated the optimal resolution from the polynomial coefficients and plotted the optimal resolution (normalized to the disk diameter) against the background size (normalized to the disk diameter); the sets of curves from the simulations which varied the object size for a fixed background and from those which varied the background size for a given object diameter agree within experimental errors and show no effects of truncation or sampling. The optimal resolution increased with increasing background size both for activity estimation and for size estimation (Fig. 5).

## DISCUSSION

The results of the simulation experiments using the ML model allow us to assess the effects of system resolution and sensitivity on quantitation from nuclear medicine images and the trade-offs involved in system design in a more complex, realistic imaging task than has been studied before.

### The Characteristics of the ML Estimator

For a high SNR, a ML estimator is expected to be unbiased; in our implementation, the bias was small relative to the variance of the estimates. The precision of our estimates scaled with $\sqrt{1/N}$ (the standard deviation of the image data) as expected. The estimates were normally distributed, and the residuals after convergence of the fitting procedure were constant in real space as well as in frequency space. These properties gave us confidence in our approach. In the high SNR conditions under which quantitation is performed, the $1/\sqrt{N}$ relationship between the precision and the number of counts in the image enables use to scale the results of our simulations to any desired system sensitivity and to predict the smallest structure which can
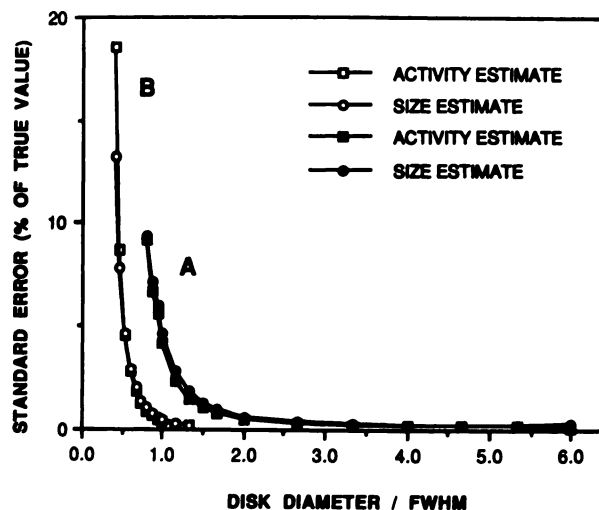


**FIGURE 2**
Standard error of disk activity and size estimates as a function of the ratio of disk diameter to FWHM of the PSF for (A) $10^6$ and (B) $10^8$ total image counts.
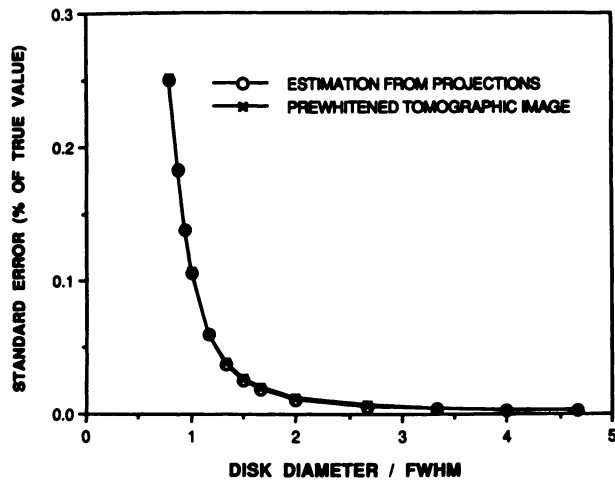
**FIGURE 3**
The standard error of disk activity estimates as a function of the ratio of disk diameter to FWHM of the PSF for ML estimation from projections versus estimation from prewhitened tomographic images.



**FIGURE 5**
The optimal resolution as a function of the ratio of background diameter-to-lesion diameter.

be quantified with a certain standard error, using a given imaging system. From the results, we are forced to conclude that the poor resolution and sensitivity of currently available SPECT systems make them inadequate for quantitation of many structures of clinical interest.

## Quantitation with ROI

Since conventional ROI peak estimates do not account for the effects of resolution, object size and background activity, they are quite biased at small lesion sizes. This bias can be reduced at the cost of precision by reducing the size of the ROI; the extreme is a one-pixel-diameter ROI, the peak estimate. Conversely, estimates from a larger ROI are more precise but less accurate, since they utilize a larger fraction of
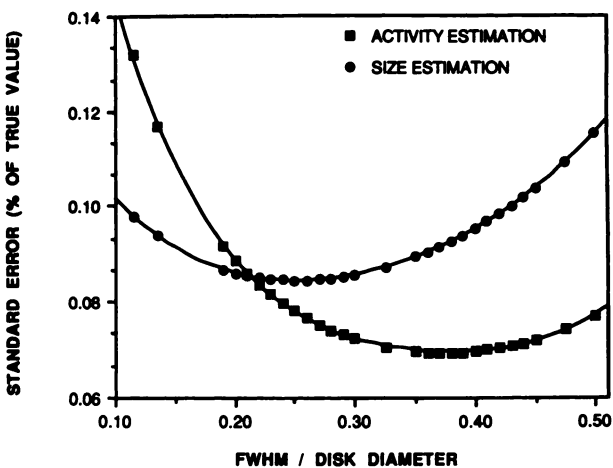


**FIGURE 4**
The dependence of standard error of disk activity and size estimates on resolution for a 20-pixel-diameter lesion and a 40-pixel-diameter background.
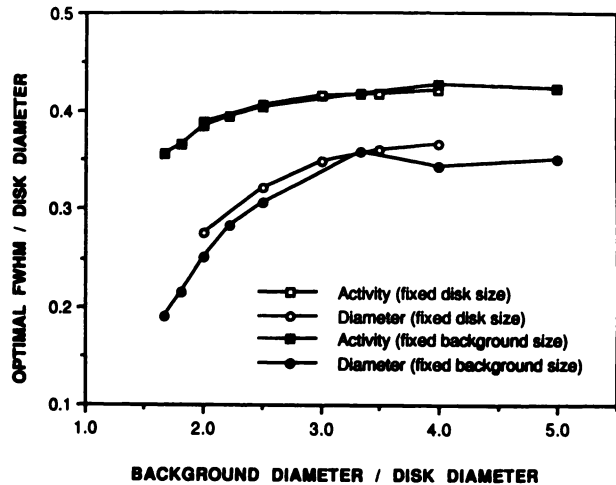
the photons emanating from the source but are more affected by reduced contrast due to limited resolution and by counts from the surrounding background. It is notable that the peak overestimates the true activity in larger lesions. When the lesion size increases to several times that of the PSF, the expected value of the maximum approaches the true activity; statistical fluctuations, however, lead to overestimation. For these reasons, ROI averages usually are not faithful estimates of the true physical quantities. In theory, the bias can be eliminated by application of recovery coefficients; this procedure, however, requires a priori information about the object size and the background activity (4). Quantitation using such independent information is a different kind of estimation task, analogous to the known-signal detection task. The distinction between these simple imaging tasks and the more complex tasks investigated here is crucial.

## Clinical Demands on Quantitation

Clinical requirements for accuracy and precision vary with the diagnostic task, being in general more stringent for absolute than for relative quantitation. Accuracy becomes crucial for relative quantitative tasks, however, if size, shape, or background activity differ among structures to be compared. Therefore, ROI methods may be inadequate even for many relative quantitative tasks in clinical nuclear medicine. For comparisons of structures of equal size, shape, and background activity, accuracy is less important than precision, and quantitative indices derived from ROI measurements may be clinically useful. Since improved precision can be obtained at the cost of accuracy, which is less important for some tasks, ROI estimates may even be preferable to more complicated estimation schemes at low count densities.

## Imaging System Requirements for Multiparameter Quantitation

The system requirements for multiparameter estimation tasks differ fundamentally from those for the simpler imaging tasks. Tasks involving only one unknown parameter, such as estimation of the activity of an object of known size without a background can best be accomplished using a system with the highest possible sensitivity, such as a well counter or whole body counter. There is no requirement for spatial resolution; the quantity of interest can be unambiguously derived from the DC information, i.e., the total number of detected counts. Spatial resolution capability is necessary for two-parameter estimation tasks, such as estimation of the activity of a structure of unknown size. The distinction between a smaller structure of higher activity and a larger structure of lower activity cannot be made using the DC component alone; the higher spatial frequency components of the object spectrum are required. Similarly, for an imaging task in the presence of a background, the feature spectrum must be distinguished from that of the background. As Hanson (28) has pointed out, the low-spatial-frequency components contain contributions from the background, the feature, and the noise. Therefore, information about the background activity depends on estimates of the feature's size and/or activity, which can only be derived from the high spatial frequencies where they can be separated. When the object size approaches the background size, the signal spectra of the object and the background become similar, and the distinction, again, lies at high spatial frequencies. These components are severely attenuated by the MTF for objects which are small compared to the system PSF. In the presence of noise, this leads to ambiguities in the data and, consequently, to negative correlations between the size and activity estimates and to rapid degradation of the precision of the ML estimates for small lesion sizes. The behavior reflects the limitations in the data for the performance in complex estimation tasks as the matched-filter SNR is a descriptor of detection performance. Our findings support the conclusion that for objects small compared to the system resolution improved resolution improves performance in complex quantitation tasks more than a large increase in image counts (Fig. 2).

Our findings with respect to the overwhelming importance of high resolution are consistent with previous studies of detection tasks. Analytical predictions (13, 28,36), computer simulation experiments (37), experimental evidence (38-40), and observer performance studies (12) have shown that an improvement of resolution moves the performance for detection or for higher-order decision tasks into a more favorable regime.

In our study, we assumed that the location of the feature was unknown, as it would be in clinical situations. We found, however, that the precision of the activity and size estimates was the same whether or not disk position was known. This is reflected in the weak correlation between estimates of position and estimates of any other parameters. These findings appear to be inconsistent with results of previous studies (10,11,31, 32) which showed that performance in detection tasks was degraded by position uncertainty. This apparent paradox can be resolved by considering the relative levels of SNR in typical detection and estimation tasks. The SNR required for estimation is much higher than the low (usually near threshold) levels of SNR typical of detection experiments where the performance in unknown-location tasks is degraded by false-positive errors which would not occur were the feature location known. At the high levels of SNR used for estimation, a clump of noise will never be mistaken for a lesion, even when location is not known.

The noise correlations in the tomographic images violate the assumption of stationary white noise implicit in the non-prewhitening estimator; ignoring these correlations degrades the performance of the estimator (7, 13,25). This degradation of performance is also observed for detection tasks (8,11,13,41). The penalty, however, can be avoided by prewhitening the image and fitting to an appropriately prewhitened model in the ML estimator (7,25). Our results indicate that the prewhitening filter adequately removes the noise correlations due to the reconstruction procedure.

Volume estimation in tomographic imaging modalities opens the possibility of measuring activity concentration without a priori assumptions about size in any dimension. The model used in this study represents a slice through a cylindrical background surrounding a cylindrical object as a tomographic imaging task. Most realistic sources of activity, however, have an axially limited extent. The axial aperture of a system is a major factor for quantitation and requires an appropriate analysis (36,42). The equivalence of estimation from prewhitened images and estimation from the projections enables us to study estimation in a three-dimensional tomographic volume by two-dimensional estimation from the projections. Since position uncertainty does not affect the other parameter estimates, a single projection image of, e.g., a centered sphere of known position, is an adequate three-parameter estimation model. Such a study would be feasible on a typical workstation. This ongoing work promises insights into the possible benefits of a truly three-dimensional quantification scheme for tomographic volume data.

## Optimization of a Collimator for Estimation of Regional Activity

The most interesting result of our collimator study is that no single optimum exists for a given object, or

even for a given set of imaging tasks; the optimum also depends on the background. This can be understood by considering, again, the frequency space representation of the model. As the background diameter increases, its spectrum narrows and the medium spatial frequencies, which contain components from both the object and the background, become available to characterize the object sufficiently, thus lowering the requirement for resolution. We expect that if the uniform background were replaced by a complex background, an increase in its size would not necessarily reduce the requirement for high resolution, since a larger background may include additional structures with high-spatial-frequency content.

At first glance, it may be surprising that the optima for activity and size estimation tasks differ, even though all parameters are estimated simultaneously. Two separate issues, however, must be considered: one is the optimal simultaneous estimation of all parameters for a given image, the other, the physical characteristics in the image favoring one parameter estimate the cost of another. (The latter question is discussed above.) The covariance matrix reflects the degree to which the worsening error in one parameter estimate influences the others, which are favored under the given circumstances. In general, the optimal collimator resolution is higher for quantitation of regional activity than for detection. (Tsui (39) reported an optimal resolution of 1.1 times the feature diameter for detection on planar images of a sphere in a background of diameter 7.7 times the feature size.) The sizing task, with an optimal FWHM of 0.25 times the disk diameter, requires even better resolution than does amplitude estimation. This is consistent with the requirement of higher spatial resolution for discriminating between tumor uptake distributions (43) and size discrimination (28) than for detection (which is closely related to a single parameter activity estimation task).

The propagation of the physician image noise to the error variance of the parameters can be estimated by methods other than computer simulation, all of which require an estimate of the covariance matrix. The complete covariance matrix cannot be derived analytically; there exist, however, first-order approximations such as the Cramer-Rao bound (7,13) and the well known first-order approximation to propagation of error analysis (15), or second-order approximations such as the Bhattacharyya bound (7). Iterative nonlinear fitting algorithms make use of a first- or second-order approximation of the covariance matrix to model the dependence of the parameters on the data. This estimate of the covariance matrix has been used to predict the precision of estimates of regional activity obtained by ML estimation in ROIs from PET images using the EM algorithm (2).

The model used in this work does not include the effects of nonstationary Poisson noise, nonstationary resolution, scatter, or attenuation. Nevertheless, it enables us to assess some general problems in quantitation, just as the matched-filter model does in detection. An advantage of the Monte Carlo approach over analytically derived bounds is that it can be modified to investigate the effects of nonstationary Poisson noise on quantitation. Resolution is of overwhelming importance for the quantitation of parameters of small structures. Although resolution of nuclear medicine imaging systems is generally non-stationary, it is approximately stationary over the extent of a small object. The effect of a perturbation of the assumption of stationary resolution with respect to the relatively large background can be directly investigated with our model but is considered minor, since the signal power of the background is low at the high spatial frequencies where the nonstationarity is reflected in the MTF.

Contributions to the image from scattered photons can be described by the system MTF and, hence, can be adequately modeled to the extent that they are stationary (44,45). The effect of the attenuation of photons by the patient is also compensated to first order by, e.g., a multiplicative correction to the geometric mean of opposing projections. For tomographic imaging, this will mainly affect the magnitude and shape of the NPS, so this effect can also be approximated in our model (22).

We conclude that our approach yields an appropriate tool for the investigation of imaging tasks in which the dependence between the image and the parameters is nonlinear, such as quantitation. Our model exactly describes the physical characteristics of the imaging system, and can, at least to first order, account for several nonstationary processes encountered in nuclear imaging; therefore, it can be used to assess the penalties imposed by these effects. The minimal model for quantitation in a clinically meaningful context is a three-parameter model of size and activity estimation of an object in an unknown background. Since position estimation is uncorrelated with these parameters, it need not be considered unless of specific interest.

## ACKNOWLEDGMENT

## REFERENCES

1. Mazziotta JC, Phelps ME, Plummer D, Kuhl DE. Quantitation in positron emission computed tomography: 5. Physical-anatomical effects. *J Comput Assist Tomogr* 1981; 5:734–743.
2. Carson RE. A maximum likelihood method for region-of-interest evaluation in emission tomography. *J Comput Assist Tomogr* 1986; 10:645–663.
3. Hoffman EJ, Huang SC, Phelps ME. Quantitation in positron emission tomography. 1. Effect of object size. *J Comput Assist*

*Tomogr* 1979; 3:299–308.

4. Kessler MK, Ellis JR, Murray E. Analysis of emission tomographic scan data: limitations imposed by resolution and background. *J Comput Assist Tomogr* 1984; 8:514–522.

5. Kojima A, Matsumoto M, Takahashi M, Hirota Y, Yoshida H. Effect of spatial resolution on SPECT quantification values. *J Nucl Med* 1989; 30:508–514.

6. Green DM, Swets JA. *Signal detection theory and psychophysics.* New York: Wiley; 1966.

7. Van Trees H. *Detection, estimation and modulation theory.* New York: Wiley; 1968.

8. Burgess AE, Wagner RF, Jennings RJ, Barlow HB. Efficiency of human signal discrimination. *Science* 1981; 214:93–94.

9. Burgess AE, Jennings RJ, Wagner RF. Statistical efficiency: a measure of human visual signal-detection performance. *J Appl Phot Eng* 1982; 8:76–78.

10. Burgess AE, Ghandeharian H. Visual signal detection. II. Signal-location identification. *J Opt Soc Am A* 1984; 1:906–910.

11. Judy P, Swensson RG, Szulc M. Lesion detection and signal-to-noise ratio in CT images. *Med Phys* 1981; 8:13–23.

12. Judy PF, Swensson RG. Detection of small focal lesions in CT images: effects of reconstruction filters and visual display windows. *Br J Radiol* 1985; 58:137–145.

13. Wagner RF, Brown DG. Unified SNR analysis of medical imaging systems. *Phys Med Biol* 1985; 30:498–518.

14. Bard Y. *Nonlinear parameter estimation.* New York: Academic Press; 1974.

15. Bevington PR. *Data reduction and error analysis for the physical sciences.* New York: McGraw-Hill; 1969.

16. Freund JE. *Mathematical statistics.* Englewood Cliffs: Prentice-Hall; 1971.

17. Press WH, Flannery BP, Teukolski SA, Vetterling WT. *Numerical recipes, the art of scientific computing.* Cambridge: University Press; 1986.

18. Huang TS. *Picture processing and digital filtering.* Berlin: Springer; 1975.

19. Carson ER, Cobelli C, Finkelstein L. *The mathematical modelling of metabolic and endocrine systems: model formulation, identification, and validation.* New York: Wiley; 1983.

20. Matis JH, Wehrly TE, Gerald KB. *The statistical analysis of pharmacokinetic data.* Berlin: Springer; 1983:1–58.

21. Shepp LA, Vardi Y. Maximum likelihood reconstruction for emission tomography. *IEEE Trans Medical Imaging* 1982; MI-1:113–122.

22. Moore SC, Kijewski MF, Mueller SP, Holman BL. SPECT image noise power: effects of nonstationary projection noise and attenuation compensation. *J Nucl Med* 1988; 29:1704–1709.

23. Riederer SJ, Pelc NJ, Chesler DA. The noise power spectrum in computed x-ray tomography. *Phys Med Biol* 1978; 23:446–454.

24. Kijewski MF, Judy PF. The noise-power spectrum of CT images. *Phys Med Biol* 1987; 32:565–575.

25. Hanson KM. Optimal object and edge localization in the presence of correlated noise. Proceedings of the Society of Photo-optical Instruction Engineers, Vol. 454, (Applications of Optical Instrumentation XII), 1984;9–17.

26. Wagner RF, Brown DG, Pastel MS. Application of information theory to the assessment of computed tomography. *Med Phys* 1979; 6:83–94.

27. Hanson KM. Detectability in computed tomographic images. *Med Phys* 1979; 6:441–451.

28. Hanson KM. Variations in task and the ideal observer. Proceedings of the Society of Photo-Optical Instrumentation Engineers, Vol. 419 (Applications of optical instrumentation in medicine XI), 1983:60–67.

29. Dennis JE, Gay DM, Welsch RE. An adaptive nonlinear least-squares algorithm. *ACM Trans Math Software* 1981; 7:348–368.

30. Nazareth L. Some recent approaches to solving large residual nonlinear least squares problems. *SIAM Rev* 1980; 22:1–11.

31. Judy PF, Swensson RG. Detectability of equally visible disks at unknown locations. [Abstract] *Radiology* 1988; 169:239

32. Swensson RG, Judy PF. Detection of noisy visual targets: models for the effects of spatial uncertainty and signal-to-noise ratio. *Percept Psychophys* 1981; 29:521–534.

33. Deans SR. *The Radon transform and some of its applications.* New York: John Wiley; 1983.

34. Ramachandran GN, Lakshminarayanan AV. Three-dimensional reconstruction from radiographs and electron micrographs: application of convolution instead of Fourier transform. *Proc Nat Acad Sci* 1971; 68:2236–2240.

35. Anger HO. *Radioisotope cameras.* New York: Academic Press; 1964:485–955.

36. Moore SC, Mueller SP, Kijewski MF, Holman BL. The axial aperture in SPECT [Abstract]. *J Nucl Med* 1986; 27:930–931.

37. Muehllehner G. Effect of resolution improvement on required count density in ECT imaging: a computer simulation. *Phys Med Biol* 1984; 30:163–173.

38. Mueller SP, Polak JF, Kijewski MF, Holman BL. Collimator selection for SPECT brain imaging: the advantage of high resolution. *J Nucl Med* 1986; 27:1729–1738.

39. Tsui BMW, Metz CE, Atkins FB, Starr SJ, Beck RN. A comparison of optimum detector spatial resolution in nuclear imaging based on statistical theory and on observer performance. *Phys Med Biol* 1978; 23:654–676.

40. Tsui BMW. A correction to "a comparison of optimum detector spatial resolution in nuclear imaging based on statistical theory and on observer performance." *Phys Med Biol* 1978; 23:1203–1205.

41. Myers KJ, Barrett HH, Borgstrom MC, Patton DD, Seeley GW. Effect of noise correlation on detectability of disk signals in medical imaging. *J Opt Soc Am A* 1985; 2:1752–1759.

42. Moore SC, Mueller SP. Inversion of the 3D Radon transform for a multi-detector point-focused SPECT brain scanner. *Phys Med Biol* 1986; 31:207–221.

43. Tsui BMW, Metz CE, Beck RN. Optimum detector spatial resolution for discriminating between tumour uptake distributions in scintigraphy. *Phys Med Biol* 1983; 28:775–788.

44. Axelsson B, Msaki P, Israelson A. Subtraction of Compton-scattered photons in single-photon emission computerized tomography. *J Nucl Med* 1984; 25:490–494.

45. Floyd CE, Jaszczak RJ, Greer KL, Coleman RE. Deconvolution of Compton scatter in SPECT. *J Nucl Med* 1985; 26:403–408.